Magnetic anisotropy of a free-standing Co monolayer and of multilayers which contain Co monolayers

G.H.O. Daalderop, P.J. Kelly, and M.F.H. Schuurmans
Philips Research Laboratories, Professor Holstlaan 4, 5656 AA Eindhoven, The Netherlands
(Received 1 March 1994)

The magnetocrystalline anisotropy energy of a free-standing [111] Co monolayer has been calculated from first principles by means of the linear muffin-tin orbital method in the atomic-spheres approximation. The results are used to analyze those obtained previously for [111] Co_1/Pd_2 and Co_1/Ag_2 multilayers. Although the magnetization of both multilayers is predicted to be oriented perpendicular to the plane of the multilayers, the easy axis of the Co monolayer is predicted to lie in plane. These results can be understood in terms of the energy bands at the high-symmetry points of the Brillouin zone only. Co_1/Pd_2 is found to have a perpendicular anisotropy because the Fermi energy is located much closer to states which have mainly Co $d_{x^2-y^2}$ and d_{xy} character than it does in the free-standing monolayer. These states are degenerate in the absence of spin-orbit coupling as a consequence of the threefold symmetry. The anisotropy energy is enhanced by the hybridization of the Pd d and Co d states and the large value of the Pd d spin-orbit coupling parameter. The smaller perpendicular magnetic anisotropy of a Co_1/Ag_2 multilayer can be attributed to the increased band filling of the Co d band structure, as well as to a smaller hybridization between Ag and Co d states.

I. INTRODUCTION

It has been established for a considerable number of [111]-oriented Co/X magnetic multilayers that the magnetization is oriented perpendicular to the multilayer planes when the cobalt layer is sufficiently thin.[1–3] An indication of the origin of this phenomenon is found in the results of measurements of the anisotropy energy density, K, carried out as a function of the thickness of the Co layers, t. The anisotropy energy density varies approximately with the inverse of the Co layer thickness and can be expressed by the relation $Kt \approx 2K_S + K_V t$. Because the demagnetization energy of bulk hcp or fcc Co in thin film form is larger than the intrinsic magnetocrystalline anisotropy energy (MAE), the volume anisotropy energy density, K_V, is negative and perpendicular magnetic anisotropy (PMA) will only occur if the interface anisotropy energy density, K_S, is sufficiently large and positive.

Various explanations for the origin of the interface anisotropy have been put forward. Néel[4] predicted that the anisotropy energy density would change markedly if the dimensions of magnetic particles were reduced to about 100 Å. He argued that the surface atoms of the particles should contribute differently to the anisotropy energy since the local symmetry of these atoms is different from that in the bulk and he developed a quantitative model based upon the assumption that the anisotropy energy can be expressed in terms of pair interaction energies between localized moments on magnetic atoms, where the parameters can be obtained from *bulk* magnetoelastic and elastic constants. Using this model for Co/X multilayers where X is a nonmagnetic atom, the interface anisotropy is implicitly expected to depend on the X atom layers *only* through their influence on the structure of the Co layers.[5]

The effect of the symmetry reduction at a surface on the anisotropy energy was also examined for an itinerant electron (band) model[6] and it was concluded that large surface contributions could also be expected for band electrons. The relationship between the reduced symmetry and enhanced anisotropy is most readily seen when the spin-orbit coupling can be treated using perturbation theory.[7] For uniaxial symmetry the anisotropy energy is proportional to ξ^2/W (instead of ξ^4/W^3 for cubic symmetry) where ξ is the spin-orbit coupling constant and W is of the order of the $3d$-band width.

More recently it has been pointed out that magnetoelastic energy could manifest itself as an interface anisotropy if the lattice misfit strain of the Co layer were inversely proportional to its thickness.[8] Experimentally however, the structures of the multilayers are not well known, so that the importance of the magnetoelastic contribution to the measured interface anisotropy is still unclear.[3,9]

Quantitative evaluations of the MAE have been reported for Co/X multilayers where X=Cu, Ag, and Pd,[10] X=Ni,[11] X=Pd, Pt, Cu, Ag, and Au,[12] X=Pd,[13] as well as for Fe/X multilayers where X=Cu, Ag, and Au.[14] From these and other[15] first-principles calculations it can be concluded that the anisotropy energy depends on the type of X atom in the (substrate) layer adjacent to the magnetic layer. Apparently Néel's theory is too simple or incomplete. In this paper a detailed explanation of the size and magnitude of the anisotropy energy of a free-standing Co monolayer and of the Co-monolayer-containing Co_1/Pd_2 and Co_1/Ag_2 multilayers will be given, based on the itinerant electron picture. The threefold symmetry of the [111] multilayers is found to be important because it gives rise to numerous twofold

0163-1829/94/50(14)/9989(15)/$06.00

degeneracies in the absence of spin-orbit coupling. The lifting of these degeneracies by the spin-orbit interaction depends on the magnetization direction and favors PMA. In order to profit from this, the Fermi level should be positioned so that a degenerate level is half-occupied. This is not so for the free-standing [111] monolayer whose magnetization is found to lie preferentially in plane. The importance of the substrate will be demonstrated by showing that for the Co_1/Pd_2 multilayer the hybridization of the Pd d levels with the Co monolayer levels positions the Fermi level very favorably at a maximum of the anisotropy energy as a function of the band filling.

The paper is organized as follows. After a brief discussion of how the anisotropy energy is calculated in Sec. II, the band structure, magnetic moments, and anisotropy energy of a free-standing Co monolayer are presented in Sec. III. These results show that the qualitative dependence of the anisotropy energy on the band filling may be obtained by considering the effect of the spin-orbit interaction on the exchange-split electronic levels at a very small number of high-symmetry points in the Brillouin zone. In Sec. IV we make use of this knowledge to carry out a detailed analysis of the anisotropy energy and to identify those factors which are most important for obtaining a large PMA. In Sec. V we consider the particular cases of the Co_1/Pd_2 and Co_1/Ag_2 multilayers and show how their anisotropy energies are related to one another and to that of the Co monolayer. Some conclusions are drawn in Sec. VI.

II. METHOD

In a previous publication[16] where the anisotropy energies of bcc Fe, hcp Co, and fcc Ni were calculated from first principles, the underlying approximations were studied at length; we refer the interested reader to this publication for a detailed discussion and further references. In this section we summarize the most important approximations and outline the procedure adopted to study a free-standing Co monolayer.

A. Computational framework

The ground state properties of the Co monolayer and of the Co/X multilayers are calculated within the local-spin-density approximation (LSDA).[17] The one-electron Kohn-Sham equations for the scalar-relativistic spin-polarized Hamiltonian are first solved self-consistently using the linear muffin-tin orbital (LMTO) method in the atomic-spheres approximation (ASA);[18] the spin-orbit interaction is treated in a subsequent step. The calculated properties of a monolayer will not be different from those of a periodic sequence of monolayers, provided that the distance between the monolayers is sufficiently large. This makes it possible to use a band-structure method that is normally used for three-dimensional crystal structures. We describe the monolayers as a sequence of [111] lattice planes of a fcc lattice. The Co layers are separated by five layers of vacuum which are filled with empty spheres serving as expansion centers for the muffin-tin orbitals. The empty spheres in the plane adjacent to the Co monolayer are denoted $E1$, in the next layer by $E2$, and in the layer furthest from the Co layer by $E3$. The stacking sequence of the spheres is chosen to be $ABCABC$, so that the lattice is close packed and has inversion symmetry. As a result of using the atomic spheres approximation and the ABC stacking sequence, the monolayer is *not* a mirror plane (the pointgroup symmetry is D_{3d}). This artifact of the ASA could be shown to be entirely negligible by performing the calculations with an $ABABAB$ stacking sequence in which case the monolayer is a mirror plane and there is no inversion symmetry.

Calculations were performed for three different lattice parameters. We denote these separate calculations as I, II, and III and they correspond to in-plane lattice constants of, respectively, 4.74 a.u., (as in a [111] plane of hcp Co), 4.92 a.u., and 5.15 a.u. (as in a [111] plane of fcc Pd). The unit of length in a.u.'s (atomic units) is the Bohr radius, $a_0 = 0.529$ Å. The corresponding atomic sphere radii are S=2.621 a.u., S=2.730 a.u., and S=2.845 a.u., respectively. S=2.845 a.u. corresponds to the in-plane lattice parameter used for calculations of the anisotropy energy of Co_n/Pd_m multilayers.[10]

The muffin-tin orbital basis contains s, p, d, and f partial waves on the Co site, s, p, and d partial waves on the empty sphere sites adjacent to the Co sites, and s and p partial waves for the other empty sphere sites. For the latter spheres this small basis is sufficient since the charge density on the empty spheres furthest from the Co monolayer (the $E3$ spheres) was negligible. Including higher order partial waves in the bases at the empty sphere sites did not influence the calculated properties. The large separation between the Co monolayers resulted in a dispersion along the $\mathbf{z}$ direction in reciprocal space which was less than 4 μeV for all energy bands within 8 eV of the Fermi energy. This very small dispersion could be safely disregarded in the calculation of all properties to be discussed here, including the anisotropy energy. As a result only two-dimensional Brillouin zone integrals had to be carried out.

B. Anisotropy energy

When both exchange interaction and spin-orbit coupling terms are included in the Hamiltonian, then the total energy depends on the direction cosines of the magnetization vector. We will define the magnetic anisotropy energy as the difference in the total energy when the magnetization is oriented along a direction $\hat{\mathbf{n}} = \hat{\mathbf{n}}(\theta, \phi)$, and when it is oriented perpendicular to the Co plane. θ and ϕ are polar coordinates with respect to a rectangular coordinate system which is defined with respect to the crystal structure. The $\mathbf{z}$ axis of the coordinate system is chosen normal to the plane of the Co monolayer, and the $\mathbf{y}$ axis is chosen along a nearest-neighbor direction. After the one electron Kohn-Sham equations for the scalar-relativistic spin-polarized Hamiltonian have been solved self-consistently the spin-orbit coupling is then

included and new Kohn-Sham one electron eigenvalues are obtained by diagonalizing the full Hamiltonian.[19] The magnetic anisotropy energy is conveniently approximated by the difference in the sums of the Kohn-Sham eigenvalues:[16,20]

$$\Delta E(\hat{\mathbf{n}}) = E(\hat{\mathbf{n}}) - E(\hat{\mathbf{z}}) = \int^{\varepsilon_F(\hat{\mathbf{n}})} \varepsilon D(\varepsilon,\hat{\mathbf{n}})d\varepsilon - \int^{\varepsilon_F(\hat{\mathbf{z}})} \varepsilon D(\varepsilon,\hat{\mathbf{z}})d\varepsilon, \quad (1)$$

where $D(\varepsilon,\hat{\mathbf{n}})$ is the density of states when the magnetization is directed along $\hat{\mathbf{n}}$. We will not consider the dependence of the magnetic anisotropy energy on the orientation of the magnetization within the plane of the monolayer, i.e., we will neglect the dependence on the azimuthal angle ϕ, as it is expected to be very small because of the high in-plane symmetry. We choose $\hat{\mathbf{n}}$ in the $\mathbf{x},\mathbf{z}$ plane (ϕ=0). In particular, we are interested in the anisotropy energy when the magnetization is rotated from $\mathbf{x}$ to $\mathbf{z}$, and this energy is denoted by $\Delta E \equiv \Delta E(\hat{\mathbf{x}})$.

Using the band structure of the Co monolayer, the Fermi energy $\varepsilon_F(q,\hat{\mathbf{n}})$, can be calculated as a function of the band filling q of this band structure.[16] An anisotropy energy curve $\Delta E(q)$ can then be obtained from Eq. (1) with $\hat{\mathbf{n}} = \hat{\mathbf{x}}$. Alternatively, we may consider the anisotropy energy curve as a function of the Fermi energy corresponding to a band filling of q states, i.e., $\Delta E(\varepsilon_F) \equiv \Delta E[\varepsilon_F(q)]$.

C. Spin-orbit coupling matrix

The dependence of the Hamiltonian on the direction of the magnetization can be implemented in several ways. The following choice is particularly convenient.[16] The exchange splitting, $b(\mathbf{r})\hat{\mathbf{n}}\cdot\boldsymbol{\sigma}$ with respect to the real space coordinate system, is diagonalized by minority-spin ("up") and majority-spin ("down") spinors which are the columns in the Wigner rotation matrices $D^{\frac{1}{2}}(\phi,\theta,0)$. By this transformation, the $\mathbf{z}$ axis of the spin coordinate system is chosen along the direction of the magnetization; the exchange splitting is given by $b(\mathbf{r})\sigma_z$, and the spin-orbit interaction by

$$D^{\frac{1}{2}\dagger}(\phi,\theta,0)\frac{\xi}{2}\mathbf{l}\cdot\boldsymbol{\sigma}D^{\frac{1}{2}}(\phi,\theta,0).$$

$b(\mathbf{r})$ is given by the functional derivative of the exchange correlation energy functional with respect to the spin density, $b(\mathbf{r}) = \delta E_{xc}/\delta m(\mathbf{r})$. More details and further references may be found in Ref. 16.

For our later analysis it is helpful to note here that the spin-orbit interaction matrix has the transparent form

$$\mathcal{H}^{SO}(\hat{\mathbf{n}}) = \frac{\xi}{2}\begin{pmatrix} \hat{\mathbf{n}}\cdot\mathbf{l} & \hat{\mathbf{n}}_\perp\cdot\mathbf{l} + \frac{1}{2}(l_- - l_+) \\ \hat{\mathbf{n}}_\perp\cdot\mathbf{l} - \frac{1}{2}(l_- - l_+) & -\hat{\mathbf{n}}\cdot\mathbf{l} \end{pmatrix}, \quad (2)$$

where $\hat{\mathbf{n}}$ is chosen in the $\mathbf{x},\mathbf{z}$ plane ($\phi = 0$); $\hat{\mathbf{n}} = (\sin\theta, 0, \cos\theta)$ and where $\hat{\mathbf{n}}_\perp$ is normal to $\hat{\mathbf{n}}$ in the $\mathbf{x},\mathbf{z}$ plane; $\hat{\mathbf{n}}_\perp = (\cos\theta, 0, -\sin\theta)$. To simplify the interpretation later on (but not for the full calculations) we will assume that the spin-orbit coupling parameters for the radial d wave functions are both energy and spin independent. Apart from the terms in the matrix elements that are independent of θ, the matrix elements between states with antiparallel spins are then identical to the matrix elements between states with parallel spins, provided that the magnetization is rotated through 90°, i.e., from $\hat{\mathbf{n}}$ to $\hat{\mathbf{n}}_\perp$. The explicit dependence of matrix elements of $\mathcal{H}^{SO}$ on the magnetization direction $\hat{\mathbf{n}}$ has been given for d orbitals in the form of tesseral harmonics in Ref. 21.

III. RESULTS

We begin this section by summarizing briefly the results of the spin-polarized (no spin-orbit coupling) calculations for Co monolayers with three different lattice parameters (Sec. III A). In Sec. III B the band structures with and without the spin-orbit interaction are compared and the most important features of the band structures identified. In Sec. III C we consider the convergence of the anisotropy energy as a function of the density of points used to calculate the single-particle eigenvalue sum in reciprocal space and show that the most important features of $\Delta E(q)$ are obtained using a very small number of sampling points in the Brillouin zone summation.

A. Magnetic moments

The number of majority- and minority-spin valence electrons in the Co atomic sphere and neighboring empty sphere are presented in Table I together with the results for the spin contribution to the magnetic moment, m_0. The magnetic moments of the monolayers are strongly enhanced with respect to hcp Co and they increase towards the value of the spin contribution to the magnetic moment of a free atom which is $3\mu_B$. There are approximately 5.3 majority-spin electrons per Co sphere in the monolayers, just as in hcp Co. The enhancement of the magnetic moments is mainly due to a transfer of 0.3–0.4 electrons with minority-spin per Co atom from the Co atomic spheres to the adjacent empty spheres which have no net magnetic moments.

It appears that the magnitude of the charges in the empty spheres decays exponentially with the distance of

TABLE I. Number of majority- ($n_\downarrow$) and minority- ($n_\uparrow$) spin electrons as well as the spin contribution to the magnetic moment (in μ_B) for hcp Co and Co monolayers with three different lattice parameters. Values are only given for the Co atomic sphere and the neighboring empty sphere ($E1$); the charges in the other empty spheres ($E2$ and $E3$) are of order 10^{-4} or less, and have therefore not been listed.

	Co $n_\downarrow$	Co $n_\uparrow$	E1 $n_\downarrow$	E1 $n_\uparrow$	m_0
hcp Co	5.28	3.72	—	—	1.57
Mono I	5.24	3.36	0.20	0.20	1.87
Mono II	5.29	3.35	0.18	0.18	1.93
Mono III	5.34	3.34	0.16	0.16	1.99

TABLE II. Orbital projected number of majority-spin and minority-spin d electrons for Co monolayer I for orbitals with angular character i, denoted by $n_{di\downarrow}$ and $n_{di\uparrow}$, respectively. The number of electrons, n_{di}, and spins, m_{di}, with angular character di as well as the deviations from spherical symmetry, $\delta\mathrm{m}_{di}$ and δn_{di}, are also given. $\sum_i \delta\mathrm{m}_{di}$ and $\sum_i \delta n_{di}$ are zero by definition.

i	m	$n_{di\downarrow}$	$n_{di\uparrow}$	m_{di}	$\delta\mathrm{m}_{di}$	n_{di}	δn_{di}
$d_{x^2-y^2}$; d_{xy}	±2	0.90	0.62	0.28	-0.09	1.52	0.02
d_{xz} ; d_{yz}	±1	0.96	0.52	0.44	0.06	1.49	-0.01
$d_{3z^2-r^2}$	0	0.96	0.52	0.43	0.06	1.48	-0.02
$\sum_i$		4.69	2.80	1.87	0.00	7.49	0.00

the empty spheres to the nearest Co atom. Whereas the empty spheres adjacent to the Co monolayer ($E1$) contain 0.3–0.4 electrons, the charge in the empty spheres in the next layer ($E2$) is less than $10^{-3}e$ or a factor of 300 smaller. In the third-layer empty sphere ($E3$) it is a factor of 10^5 smaller. The magnetic moment of the $E1$ empty spheres adjacent to the Co layer is of the order of $10^{-3}\mu_B$.

The symmetry of a [111] monolayer is such that the spin density $m(\mathbf{r})$ [and also the electron density $n(\mathbf{r})$] has the form

$$\mathrm{m}(\mathbf{r}) = \mathrm{m}_{00}(r)Y_0^0(\hat{\mathbf{r}}) + \mathrm{m}_{20}(r)Y_2^0(\hat{\mathbf{r}}) + \mathrm{m}_{40}(r)Y_4^0(\hat{\mathbf{r}}) + \mathrm{m}_{60}(r)Y_6^0(\hat{\mathbf{r}}) + \mathrm{m}_{66}(r)Y_6^6(\hat{\mathbf{r}}) + \cdots . \quad (3)$$

The s- and p-like electrons contribute negligibly to the spin density; we therefore only consider the contributions of the d electrons to $\mathrm{m}(\mathbf{r})$ and further, only the diagonal contributions of the density matrix $n_{li\sigma;l'i'\sigma'}$ which, in the absence of spin-orbit coupling, is diagonal in the spin indices. For spherical harmonics $i = m = -2,-1,0,1,2$; for real cubic harmonics $i = d_{x^2-y^2}$, d_{xy}, d_{xz}, d_{yz}, or $d_{3z^2-r^2}$. We use the shorthand notation $n_{li\sigma} \equiv n_{li\sigma;li\sigma}$ for the number of electrons with orbital character li and spin σ. Values of $n_{di\sigma}$ and of $\mathrm{m}_{di} = n_{li\downarrow} - n_{li\uparrow}$ are given in Table II for the Co monolayer with lattice constant I. The total d spin, $\mathrm{m}_d = \sum \mathrm{m}_{di} = 1.87$ is almost identical to m_0 from Table I confirming that the sp (and f) contribution to the spin density is negligible. The d spin density deviates strongly from spherical symmetry. If it were spherically symmetric, then m_{di} would be equal to $\mathrm{m}_d/5 = 0.37$ and $\mathrm{m}(\mathbf{r}) = \phi_d^2(r)\,\mathrm{m}_0/4\pi$ where $\phi_d(r)$ is the appropriate d radial wave function. The deviations of m_{di} from the value giving the same total spin but a spherically symmetric spin density, $\delta\mathrm{m}_{di}$ is given in Table II. The first nonspherical term in the spin density, $\mathrm{m}_{20}(r)Y_2^0(\hat{\mathbf{r}})$, can be written as $\phi_d^2(r)\sqrt{\frac{5}{49\pi}}\Delta\mathrm{m}Y_2^0(\hat{\mathbf{r}})$ where

$$\Delta\mathrm{m} = \mathrm{m}_{d_{3z^2-r^2}} + \frac{1}{2}(\mathrm{m}_{d_{xz}} + \mathrm{m}_{d_{yz}}) - (\mathrm{m}_{d_{x^2-y^2}} + \mathrm{m}_{d_{xy}}) = 0.31. \quad (4)$$

The value of the analogous quantity Δn for the electron density is only -0.06. Thus the majority-spin density is strongly prolate having the shape of a cigar oriented along the direction normal to the plane of the monolayer while the minority-spin density is strongly oblate and has the shape of a pancake in the plane of the monolayer. The two effects cancel for the electron density but add up for the spin density. The origin of this effect can be understood very simply in terms of the band structure and the corresponding partial state densities $D_{di\sigma}(\varepsilon)$.

B. Band structure

The band structure $\varepsilon_{n\mathbf{k}\sigma}$ along the high-symmetry lines Γ-K-M-Γ in the two-dimensional BZ is shown in Fig. 1 for the majority-spin (dashed curves) and minority-spin bands (solid curves). Here n is the band index and $\mathbf{k}$ is the two-dimensional Bloch wave vector. The results shown are for the Co monolayer with lattice parameter I. Only the energy range of the d bands has been shown and the Fermi energy (corresponding to nine valence electrons) is denoted by the horizontal solid line. At the high-symmetry points the dominant angular dependence of the d partial waves contributing to the eigenstates is indicated. Taking an average of the exchange splitting, $\Delta\varepsilon_{n\mathbf{k}} = \varepsilon_{n\mathbf{k}\downarrow} - \varepsilon_{n\mathbf{k}\uparrow}$, over the d bands

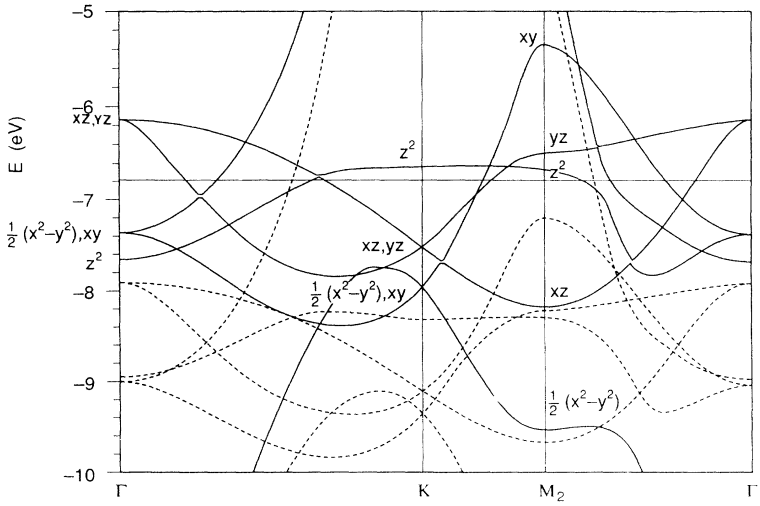

FIG. 1. Majority-spin (dashed) and minority-spin (solid) band structure of Co monolayer I along the high-symmetry lines of the two-dimensional Brillouin zone in the energy range of the d bands. The Fermi energy is denoted by the horizontal line. The predominant character of the minority-spin eigenstates at the high-symmetry points is indicated.

at the points of high symmetry, we find a value of 1.6 eV corresponding to a Stoner exchange parameter,

$$I_{xc} = \frac{\overline{\Delta\varepsilon}}{m_d},$$

of 0.86 eV where the d spin moment $m_d = 1.87$. This value of I_{xc} is about 15% smaller than the values calculated for bulk Co;[22] the same seems also to be true for a Ni monolayer.[23] The exchange splitting is largest ($\sim$ 1.8 eV) at the top of the d-band complex and smallest ($\sim$ 1.3 eV) at the bottom reflecting the energy dependence of I_{xc}.[22] Because the radial d wave function contracts with increasing energy, the exchange integral increases (decreases) going towards the top (bottom) of the d band. Corresponding to this energy dependence, the width of the minority-spin d band is larger than that of the majority-spin d band.[23]

The d band which is singly degenerate at Γ, which disperses upwards in the directions of K and M and which is essentially flat between K and M, has mainly $d_{3z^2-r^2}$ character ($l = 2, m = 0$). The small dispersion is caused by the small overlap of $d_{3z^2-r^2}$ orbitals on neighboring Co atoms. In contrast, the bands with mainly $d_{x^2-y^2}$ and d_{xy} character ($l = 2, |m| = 2$) show the largest dispersion. The dispersion of the bands with d_{xz} and d_{yz} character ($l = 2, |m| = 1$) is intermediate. Because the plane of a monolayer is a mirror plane, the eigenstates of the bands are either odd in z (with d_{xz}, d_{yz} character, $|m| = 1$) or even in z ($|m| = 0, 2$). These eigenstates belong to different representations and do not hybridize;[24] the d-band structure can be simply calculated by diagonalizing a 2×2 and a 3×3 matrix.[23]

The orbital ($|m|$) projected densities of states corresponding to the band structure shown in Fig. 1 are shown in Fig. 2 for the majority-spin (dashed curves) and minority-spin (solid curves) states. The bandwidths for the three types of orbitals differ considerably as a consequence of the directionality of the orbitals. The $m = 0$ density of states is extremely narrow and exhibits a peak originating in the nearly dispersionless portion of the band around K-M. The $|m| = 1$ density of states consists of two peaks; the bonding states are located in a region of the Brillouin zone away from Γ but including K and M; the antibonding states in a region containing Γ and M but not K. The $|m| = 2$ density of states is very broad, without any pronounced structure.

The origin of the different spatial distribution of the majority- and minority-spin densities now becomes apparent. The $m = 0$ and $|m| = 1$ majority-spin states are completely filled. The large dispersion of the $|m| = 2$ states combined with the hybridization with the free electronlike states leads to a tail in the majority-spin density of states with $|m| = 2$ character above the Fermi energy; all the holes in the majority-spin bands have $|m| = 2$ character so that $\Delta n_\downarrow = 0.13$ where Δn_σ is defined analogously to Δm in Eq. (4). For the minority-spin states, the situation is reversed. There are peaks in the minority-spin densities of states for both $m = 0$ and $|m| = 1$ above the Fermi energy whereas the broad peaks in the $|m| = 2$ density of states are below ε_F. Thus $\Delta n_\uparrow = -0.19$.

In Fig. 3 the band structure including spin-orbit coupling is shown along the high-symmetry lines Γ-K-M_2-Γ-M_1, where $\hat{\mathbf{n}} = \hat{\mathbf{x}}$ (dashed curves) and $\hat{\mathbf{n}} = \hat{\mathbf{z}}$ (solid curves). Here $M_2 = \frac{1}{2}\mathbf{G}_2$ and $M_1 = \frac{1}{2}\mathbf{G}_1$, where $\mathbf{G}_{1,2}$ are the reciprocal lattice vectors and $\mathbf{G}_2 \parallel \mathbf{x}$. These M points are equivalent in the absence of spin-orbit coupling. The most obvious, *visible* effect upon rotating $\hat{\mathbf{n}}$ is the changed splitting of energy bands which were degenerate (either accidentally or by symmetry) in the

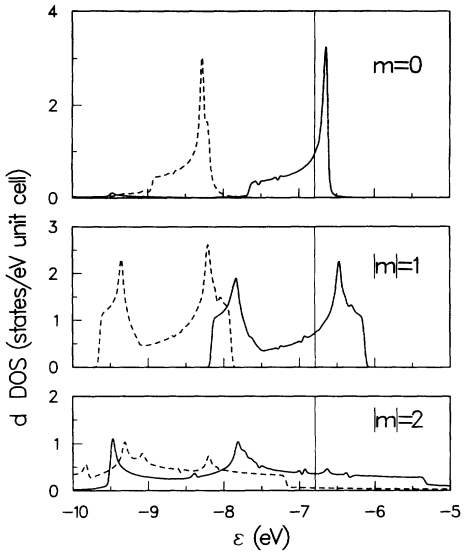

FIG. 2. Majority- (dashed) and minority-spin (solid) orbital projected d density of states with $m = 0$ (top), $|m| = 1$ (middle), and $|m| = 2$ (bottom), corresponding to the band structure shown in Fig. 1. The density of states was calculated using 816 irreducible **k** points and broadened using a Gaussian with width 0.05 eV. The Fermi energy corresponding to an occupancy of nine electrons is indicated by the vertical lines.

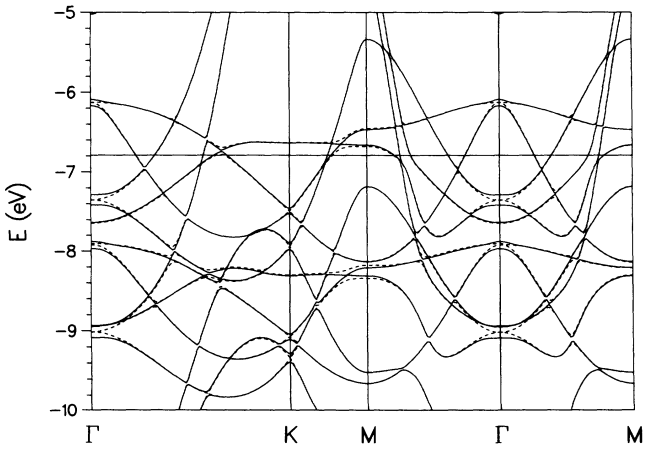

FIG. 3. Band structure of Co monolayer I along high-symmetry lines of the two-dimensional Brillouin zone, where spin-orbit coupling has been included. Solid curve, magnetization parallel to **z**; dashed curve, parallel to **x**. M_1 and M_2 are the M points along the reciprocal lattice vectors $\mathbf{G}_1$ and $\mathbf{G}_2$, respectively, where $\mathbf{G}_2 \parallel \mathbf{x}$.

absence of spin-orbit interaction. However, *all* energy bands change on a scale of 10^0–10^1 meV and this will be important when we investigate the anisotropy energy.

C. Anisotropy energy

The anisotropy energy of a Co monolayer is shown as a function of the band filling in Fig. 4 for the three different lattice parameters I, II, and III; it has been smoothed using a Gaussian with a width $\alpha = 0.2$ eV, whereby the function $\Delta E(\varepsilon)$ is replaced by

$$\frac{1}{\alpha\sqrt{\pi}} \int_{-\infty}^{\infty} \Delta E(\varepsilon') e^{-(\frac{\varepsilon-\varepsilon'}{\alpha})^2} d\varepsilon'.$$

The demagnetization energy, which is ~0.1 meV per Co, is negligible on the scale of the figure and has therefore been omitted. Whereas a perpendicular anisotropy was calculated for Co_1/Pd, Co_1/Ag, and Co_1/Cu multilayers,[10] an in-plane anisotropy is seen to be found for a Co monolayer for a Fermi energy corresponding to nine electrons. Although the anisotropy energy depends quite strongly on the lattice parameter and the position of the actual Fermi energy, the functional form of *all* three anisotropy energy curves is very similar. There are four distinct regions: for a band filling between 8.5 electrons and a filled d band, the anisotropy energy is negative favoring an in-plane magnetization; for a band filling between about 5.5 and 8.5 electrons, the anisotropy energy is positive corresponding to perpendicular magnetization; for a band filling of between 3 and 5.5 electrons, the anisotropy energy is again negative; for a smaller band filling, the anisotropy energy is small and slightly positive. These are the main features which we will seek to understand in the next section. To do so, it is sufficient to analyze one case only and we will discuss the monolayer with lattice parameter I.

In Fig. 5 the anisotropy energy at a band filling of 8.2, 9.0, and 9.4 electrons is shown as a function of the area s of the surface element used to perform the integration over the two-dimensional BZ. The corresponding number of divisions of the reciprocal lattice vectors is denoted at the top of the figure. Using 96 divisions, the anisotropy energy is converged to within 50 μeV. Where

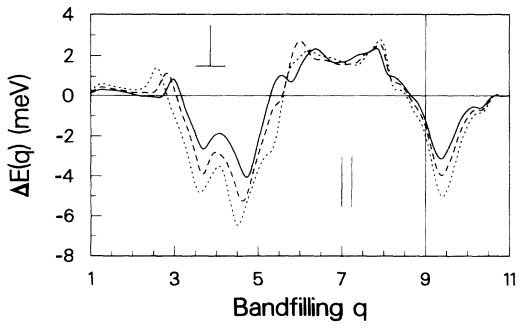

FIG. 4. Anisotropy energy vs band filling for Co monolayers at three different lattice parameters: monolayer I, solid curve; II, dashed curve; and III, dotted curve.

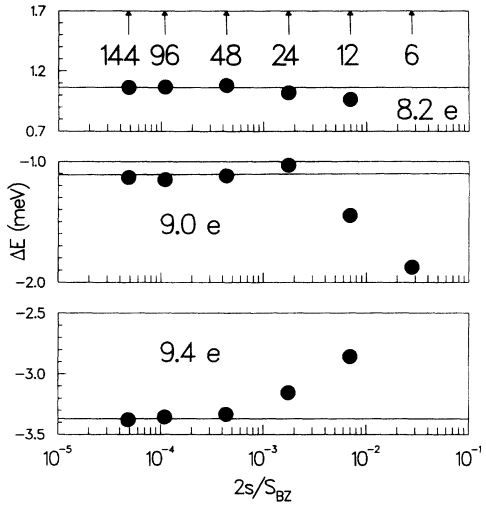

FIG. 5. Convergence of the anisotropy energy of monolayer I at three band fillings, 8.2, 9.0, and 9.4 electrons, as a function of the area, s, of the triangular surface element used to perform the two-dimensional BZ integral, given as a fraction of the total area of the 2D BZ, S_{BZ}. The number of divisions of the reciprocal lattice vectors corresponding to each surface element is indicated at the top of the figure. The horizontal lines were obtained by a least squares fit through the data points using a weight $1/s$ for each data point and denote the converged value.

the anisotropy energy does not vary much with the band filling, e.g., at a band filling of 8.2 electrons, the convergence is even better. We note that even though an accurate value of the anisotropy energy can only be calculated with a quite dense integration mesh, the sign and the order of magnitude are already obtained using a small number of **k** points.

Assuming that the anisotropy energy is an analytical function of the direction cosines of the magnetization, it follows from the symmetry of an hexagonal lattice that the anisotropy energy can be expanded as $\Delta E(\hat{\mathbf{n}}) \approx K_2 \sin^2\theta + K_4 \sin^4\theta = \Delta E(\theta)$. K_2 and K_4 are second- and fourth-order anisotropy constants, respectively. Sixth- and higher-order anisotropy constants (which also depend on ϕ) have been ignored. The magnitude of K_4 has been investigated for the band fillings given above. In Fig. 6, $\Delta E(\theta)/\sin^2\theta$ is shown as a function of $\sin^2\theta$. K_2 is given by the intercept with the vertical axis, K_4 is given by the slope of the line. For the band fillings of 8.2 and 9.4 electrons, K_4 is less than 3% of the value of K_2. This is of the same order of magnitude as the numerical accuracy of the calculation. At a band filling of 9.0 electrons the expansion does not appear to be adequate. We have not investigated this further, but it may be related to the existence of accidental degeneracies along the high-symmetry lines Γ-K and K-M.[25] From arguments based on perturbation theory,[7] one would expect the higher order anisotropy constants to be smaller than K_4.

In Fig. 7 the anisotropy energy curve calculated for the Co monolayer I using a small number of **k** points is compared to that obtained from a calculation employing

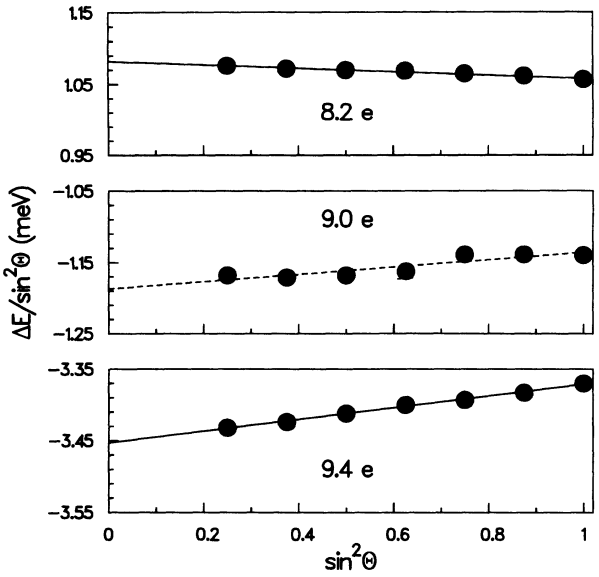

FIG. 6. $\Delta E(\theta)/\sin^2\theta$ as a function of $\sin^2\theta$. ΔE was calculated using 144 divisions of the reciprocal lattice vectors. The second order anisotropy constant K_2 is given by the intercept of the line, obtained by a least squares fit, with the vertical axis. The fourth-order anisotropy constant K_4 is given by the slope of the line. For a band filling of 9.0 electrons, the expansion does not appear to be adequate.

a much larger number; the solid curve was calculated using 144 divisions of the reciprocal lattice vectors, the dashed curve using only 6. In the latter calculation only seven irreducible $\mathbf{k}$ points are used if $\hat{\mathbf{n}} = \hat{\mathbf{z}}$. The curve has been broadened using a Gaussian with a width of 0.2 eV to smear the discrete energies into bands. We will now show that the most important qualitative features of the anisotropy energy curve of a monolayer can be understood by analyzing the eigenstates and energies at an even smaller number of $\mathbf{k}$ points, namely, the high-symmetry points Γ, K and M *only.*[26]

The contributions to the anisotropy energy from these $\mathbf{k}$ points are shown in the top three panels of Fig. 8. The anisotropy energy at each $\mathbf{k}$ point is broadened using a

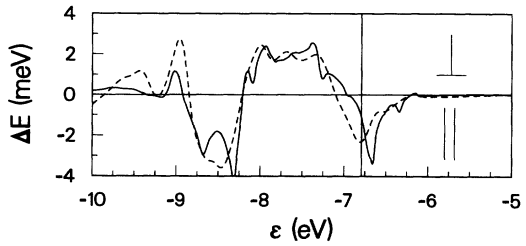

FIG. 7. Anisotropy energy curve as a function of an energy corresponding to variable band filling of the band structure, calculated using two different Brillouin zone samplings. The solid and dashed curves were calculated with 144 divisions and 6 divisions of the reciprocal lattice vectors, respectively. The dashed curve has been broadened using a Gaussian with a width of 0.2 eV. The actual Fermi energy is denoted by the vertical line.

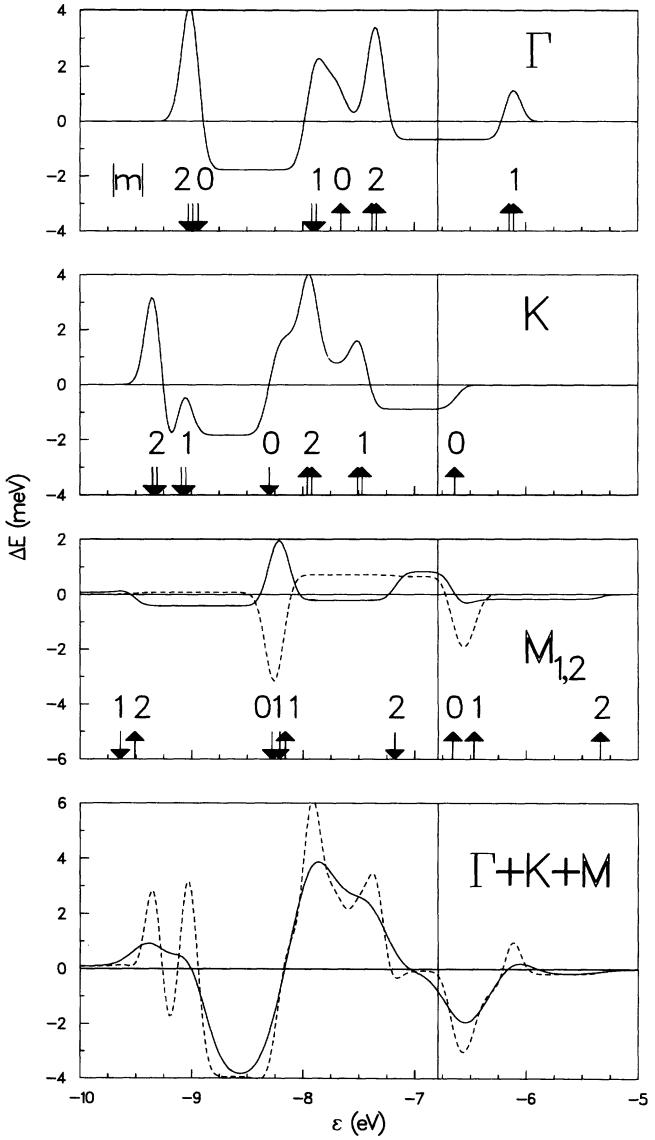

FIG. 8. Top three panels: anisotropy energy contributed by Γ, K, and M_1 (solid curve) and M_2 (dashed curve), as a function of the energy corresponding to variable band filling of the fixed band structure. The weight factor, $w_{\mathbf{k}}$, is included. The arrows indicate the position of the energy levels; a double arrow is used to denote doubly degenerate eigenstates. Upward (downward) pointing arrows indicate minority- (majority-) spin eigenstates. The dashed curve in the bottom panel is the result of adding the contributions of these $\mathbf{k}$ points. The solid curve was obtained by broadening the dashed curve using a Gaussian with a width of 0.4 eV. The actual Fermi energy is indicated by the vertical lines.

Gaussian with a width of 0.2 eV, and multiplied with a weight factor $w_{\mathbf{k}}$. The total anisotropy energy curve, shown in the bottom panel, is obtained by summing the weighted contributions from each $\mathbf{k}$ point. The weight factors for the $\mathbf{k}$ points Γ, K, and M are determined by their number density in the BZ. If $\hat{\mathbf{n}} = \hat{\mathbf{x}}$ (parallel to the reciprocal lattice vector $\mathbf{G}_2$), the two K points in the BZ,

$\frac{1}{3}(\mathbf{G}_1+\mathbf{G}_2)$ and $\frac{2}{3}(\mathbf{G}_1+\mathbf{G}_2)$, are equivalent. One of the M points, $M_2=\frac{1}{2}\mathbf{G}_2$, is not equivalent to the other two M points, $\frac{1}{2}\mathbf{G}_1$ and $\frac{1}{2}(\mathbf{G}_1+\mathbf{G}_2)$, denoted by M_1. The weight factors for the special points Γ, K, M_1, and M_2 are then chosen as 1/6, 1/3, 1/3, and 1/6, respectively.

The arrows in Fig. 8 indicate the positions of the energy levels at each $\mathbf{k}$ point, and a double arrow denotes degenerate energy levels (in the absence of spin-orbit interaction). Upward (downward) pointing arrows denote minority- (majority-) spin eigenstates. The eigenstates have mainly d character, and the predominant magnetic quantum number character, $|m|$, of the d partial wave is also indicated. The contributions from M_1 and M_2 are indicated by the solid and the dashed curves, respectively. In the bottom panel the dashed curve gives the sum of the contributions from the individual $\mathbf{k}$ points; the solid curve is obtained by an additional broadening with a Gaussian with a width of 0.4 eV. The anisotropy energy curve calculated from the high-symmetry points only is seen to exhibit all the important qualitative features obtained in the full calculation (see Fig. 7), which is what we set out to demonstrate. In the following section we proceed to a detailed analysis of the contributions from Γ, K, and M.

IV. ANALYSIS OF THE ANISOTROPY ENERGY

At a high-symmetry $\mathbf{k}$ point, two types of contributions to the anisotropy energy can be distinguished. One contribution comes from the splitting by the spin-orbit interaction of partly occupied orbitally degenerate levels and results in a lowering of the total energy. Since the spin-orbit splitting depends on the magnetization direction, so does the total energy. "True" twofold degeneracies only exist at the high-symmetry points Γ and K. Along lines of high symmetry, accidental degeneracies occur as a result of the existence of different irreducible representations; the accidental degeneracies which occur along K-M at $\varepsilon\sim-6.7$ eV are found to be particularly important for a quantitative evaluation of the anisotropy energy but neglecting them will not affect our qualitative conclusions. For the "true" degeneracies, the corresponding eigenstates will involve partial waves with (l,m) and $(l,-m)$ character, where $l=2$ and $m=2$ or $m=1$. The spin-orbit coupling splits the degenerate energy bands by $m\xi|\cos\theta|$. If perturbative coupling to other bands is neglected (to be discussed below), the degeneracy is not lifted when $\hat{\mathbf{n}}=\hat{\mathbf{x}}$ ($\theta=\frac{\pi}{2}$). True degeneracies at the Fermi energy therefore give a contribution to the anisotropy energy which favors the perpendicular orientation (θ=0).

The second type of contribution is due to the spin-orbit interaction coupling eigenstates ψ_i and ψ_j with energies ε_i below the Fermi energy and ε_j above the Fermi energy. If the level splitting $\Delta_{ij}=\varepsilon_i-\varepsilon_j$ is much larger than the spin-orbit coupling parameter ξ one can use perturbation theory to deduce the contribution to the anisotropy energy. The contribution from each pair of states is given by $w_{\mathbf{k}}\Delta E_{ij}$, where

$$\Delta E_{ij}=\frac{1}{\Delta_{ij}}\left(|\mathcal{H}_{ij}^{\mathrm{SO}}(\hat{\mathbf{x}})|^2-(|\mathcal{H}_{ij}^{\mathrm{SO}}(\hat{\mathbf{z}})|^2\right) \tag{5}$$

and $\mathcal{H}_{ij}^{\mathrm{SO}}(\hat{\mathbf{n}})\equiv\langle\psi_i|\mathcal{H}^{\mathrm{SO}}(\hat{\mathbf{n}})|\psi_j\rangle$. This contribution to the anisotropy energy can favor either a perpendicular orientation, or an in-plane orientation of the magnetization, depending on the spins and symmetries of the states i and j. In the bottom panels of Figs. 9–11 for Γ, K, and M_2, respectively, the contribution ΔE_{ij} to the anisotropy energy from each pair of eigenstates ε_i and ε_j, calculated using perturbation theory, is denoted by a bar connecting the eigenstates. The height of each bar is drawn proportional to ΔE_{ij}. A coupling between two eigenstates favoring an in-plane (perpendicular) orientation of the magnetization is indicated by horizontally (vertically) shaded bars. The top panels of Figs. 9–11 were calculated by full (numerical) diagonalization of the Hamiltonian, and contain the contribution of both the spin-orbit split degenerate levels at the Fermi energy, accounting for most of the structure in the panels, as well as the contributions of the spin-orbit coupled states lying energetically on opposite sides of the Fermi energy.

Let us illustrate with an example how perturbative

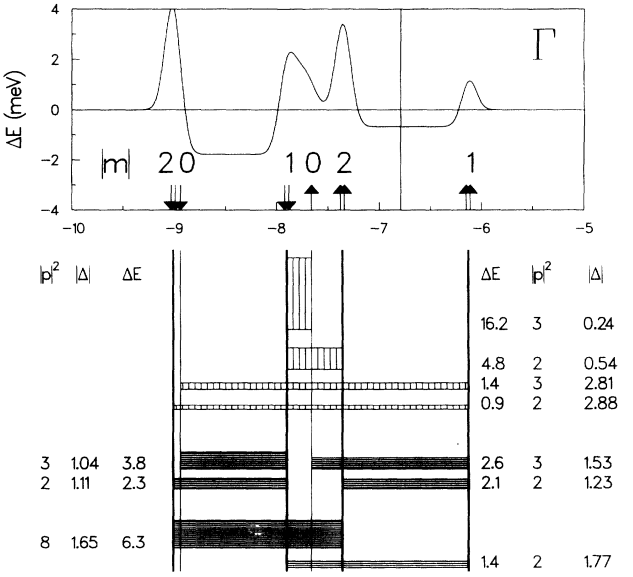

FIG. 9. Anisotropy energy contributed by Γ as a function of the energy, analyzed using perturbation theory in the bottom panel. The anisotropy energy ΔE_{ij} contributed by each pair of states i and j is proportional to the thickness of the bars connecting these states. Horizontally (vertically) shaded bars indicate in-plane (perpendicular) contributions to the anisotropy energy. Perpendicular contributions originating from degenerate eigenstates have not been indicated in the bottom panel of the figure. Only couplings with $\Delta E_{ij}>1$ meV have been indicated. Both ΔE_{ij} (in meV), the separation in energy Δ_{ij} (in eV) and $|p_{ij}|^2$ have been indicated (the labels ij have been omitted in the figure). A spin-orbit coupling parameter ξ of 72 meV was assumed in the analysis. Note that the solid curve in the top of the figure was calculated by diagonalization of the Hamiltonian. The actual Fermi energy is denoted by the vertical lines at −6.8 eV.

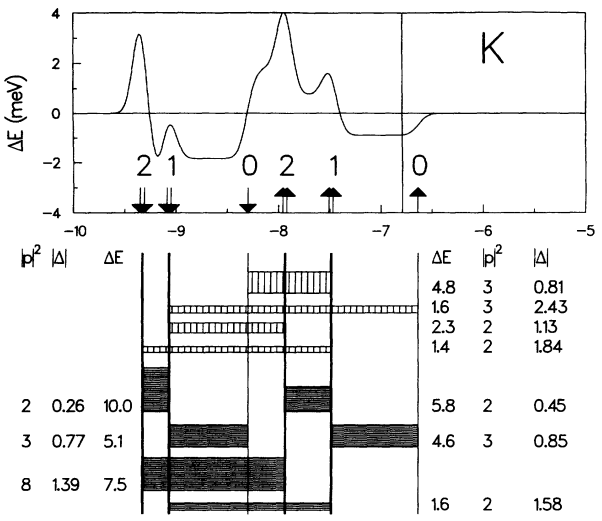

FIG. 10. Anisotropy energy contributed by K as a function of the energy, analyzed using perturbation theory in the bottom panel. See caption to Fig. 9.

coupling between states on either side of the Fermi energy can give a large contribution to the anisotropy energy. Consider the $|m\sigma\rangle = |0\downarrow\rangle$ and $|\pm 1\uparrow\rangle$ eigenstates at Γ. The relevant matrix elements for the anisotropy energy are

$$\langle 0\downarrow|\mathcal{H}^{\mathrm{SO}}(\hat{\mathbf{n}})|\pm 1\uparrow\rangle = \frac{\xi}{2}\langle 0| - \sin\theta l_z + \cos\theta l_x + i l_y|\pm 1\rangle$$
$$= \frac{\xi}{2}(\cos\theta \mp 1)\sqrt{\frac{3}{2}}.$$

Therefore,

$$\Delta E_{0\downarrow,+1\uparrow} + \Delta E_{0\downarrow,-1\uparrow} = |p|^2 \frac{\xi^2}{4\Delta_{0\downarrow,\pm 1\uparrow}},$$

where $|p|^2 = 2\times\frac{3}{2}$, $\Delta_{0\downarrow,\pm 1\uparrow} = -2.81$ eV, and $\xi = 72$ meV. Despite the fact that Δ_{ij} is larger than the d-band width, the contributed anisotropy energy is large, of the order of $w_\Gamma \times 1.4$ meV $= 0.23$ meV and favors a perpendicular magnetization. In the following, each high-symmetry point will be discussed briefly.

A. Γ

The five d states (per spin) split at Γ into a singly degenerate state with $m = 0$ character and two doubly degenerate states with $m = \pm 2$ and $m = \pm 1$ character, respectively; see Figs. 1 and 9. The $m = 0$ and $m = \pm 2$ states have bonding character and are well separated in energy from the antibonding $m = \pm 1$ states. Because the smallest exchange splitting, which is 1.3 eV for the $m = 0$ states, is larger than the energy spread of 1.1 eV for the majority-spin states (1.5 eV for the minority-spin states), there is no overlap between the uppermost $\downarrow$-spin and lowermost $\uparrow$-spin states at Γ. The spin-orbit interaction between the states at Γ is such that an in-plane magnetization is favored for a Fermi energy located between the even ($m = 0, \pm 2$) and odd ($m = \pm 1$) states of either spin. A perpendicular magnetization is favored for Fermi energies at the top, the middle, or the bottom of the energy range shown in Fig. 9. This behavior can be simply understood by referring to the form of the spin-orbit interaction in Eq. (2) and the lower panel of Fig. 9.

(i) The coupling $\frac{\xi}{2}\hat{\mathbf{n}}\cdot\mathbf{l}$ between even and odd states of the same spin is zero if $\hat{\mathbf{n}} = \hat{\mathbf{z}}$ and nonzero if $\hat{\mathbf{n}} = \hat{\mathbf{x}}$. Thus this interaction favors an in-plane magnetization for Fermi energies located in between even and odd states of the same spin.

(ii) The coupling between even states of opposite spin (and also odd states of opposite spin) is nonzero if $\hat{\mathbf{n}} = \hat{\mathbf{x}}$. Thus this interaction also favors an in-plane magnetization for Fermi energies located in between even (and odd) states of opposite spin.

(iii) The coupling between even states of one spin and odd states of the opposite spin is nonzero if $\hat{\mathbf{n}} = \hat{\mathbf{z}}$. The contribution from even $\downarrow$-spin states interacting with odd $\uparrow$-spin states is dominated by the large denominator and very small. By contrast, the odd $\downarrow$-spin states are very close in energy to the even $\uparrow$-spin states and for Fermi energies in between the $\downarrow$-spin and $\uparrow$-spin states there is a large contribution favoring a perpendicular magnetization.

(iv) The remaining contribution coming from the lifting of degeneracies also favors a perpendicular magnetization, so that for a Fermi energy between -7.4 and -7.9 eV, contributions (iii) and (iv) prevail. The degeneracy-lifting contribution also dominates at the bottom of the $\downarrow$-spin states and at the top of the $\uparrow$-spin states.

B. K

A similar analysis can be carried out for the anisotropy energy curve of the K point, shown in Fig. 10. The conditions for the existence of nonzero couplings are the same as for the Γ point; the principal difference lies in the different positions of the energy levels. The smallest exchange splitting at K (1.4 eV for the $m = \pm 2$ states) is larger than the energy spread of the $\downarrow$-spin states (1.0 eV) so there is again no overlap between the $\downarrow$-spin and $\uparrow$-spin states. At the K point, the five d states (per spin) split into a singly degenerate state with $m = 0$ character and two doubly degenerate states with $m = \pm 1$ and $m = \pm 2$ character, respectively. As a consequence of the phase factor introduced in the Bloch wave, the $m = \pm 1$ states now have mainly bonding character while the $m = 0$ state is antibonding. The $m = \pm 2$ states are strongly bonding. Thus for each spin, the lowest eigenstates have $m = \pm 2$ and $m = \pm 1$ character and the highest antibonding eigenstate has $m = 0$ character. If the Fermi energy is situated in the lower part of each spin subband, the degenerate states will favor a perpendicular orientation of the magnetization which, however, is reduced by the coupling between $m = \pm 2$ and $m = \pm 1$ orbitals. In the middle of the spin subband, an in-plane orientation is favored, as at Γ. The couplings between the uppermost majority-spin states and the lowermost minority-spin states favor a perpendicular orientation of the magnetization for a Fermi energy lying between -7.5

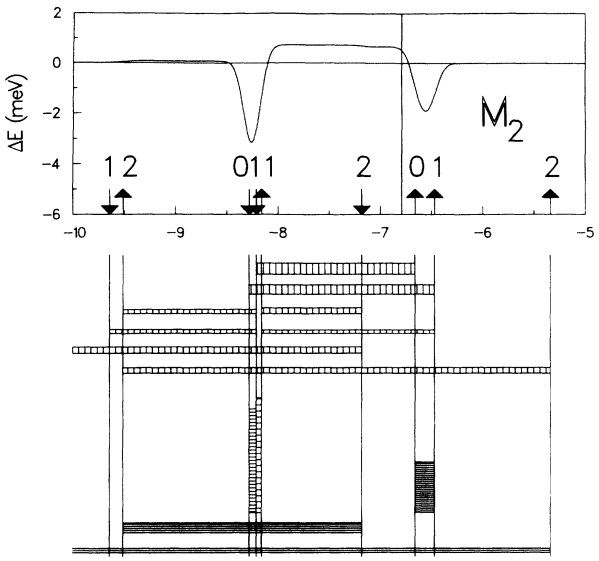

FIG. 11. Anisotropy energy contributed by M_2 as a function of the energy, analyzed using perturbation theory in the bottom panel. See caption to Fig. 9.

and -8.3 eV coinciding with the position of the degenerate $m = \pm 2$ and $m = \pm 1$ $\uparrow$-spin states. There is therefore a strong preference for perpendicular magnetization in this energy range.

C. M

The situation at the M points is more complex, as can be seen from Fig. 11. No true degeneracies exist because all representations at the M point are one dimensional. We simply note here that all couplings cancel to a large extent, except where eigenstates are close in energy.

Thus the mechanisms by which perpendicular anisotropy occurs are (a) through the lifting of degeneracies at Γ and K and (b) through the couplings by the spin-orbit interaction of even states of one spin with odd states of the opposite spin. The latter type of contribution is important when, as a result of a decrease in the bandwidth and an increase in the exchange splitting, the top of the majority-spin subband and the bottom of the minority-spin subband are close in energy, and the actual Fermi energy is located at the bottom of the minority-spin band. There is then a large contribution to the magnetic anisotropy energy favoring perpendicular magnetization from the coupling by the spin-orbit interaction of even states with odd states of the opposite spin. This situation can occur in layered structures, when the number of equivalent nearest neighbors is small (narrow bandwidth), and when the center of the d bands of the nonmagnetic transition metal element is sufficiently low in energy. As an example of where this occurs, we have considered compounds with the AuCu ($L1_0$) structure, where the constituent elements are Fe or Co and Pd or Pt.[27] The perpendicular orientation is then favored if the Fermi energy is at, or above, the top of the majority-spin subband and in the bottom of the minority-spin subband.

In the middle of each spin subband, an in-plane anisotropy is generally favored, because the couplings between bonding and antibonding eigenstates within one-spin subband favor the in-plane orientation. The anisotropy energy is thus expected to oscillate with the band filling. On general grounds this has been proven for a tight-binding d band.[28]

V. ANISOTROPY ENERGY OF CO_1/X_2 MULTILAYERS

A. Co_1/Pd_2

In an earlier publication, we calculated the magnetic anisotropy energy for a number of Co_n/Pd_m multilayers and found the largest perpendicular anisotropy energy for the Co_1/Pd_2 multilayer.[10] In this section we will use the results of the previous section to relate the anisotropy energy of the Co_1/Pd_2 multilayer to that of the free-standing Co monolayer. We will demonstrate that, just as in the case of the monolayer, the dependence of the anisotropy energy on the band filling can be understood by considering the contributions from the high symmetry points only.[26] For the multilayer, the dispersion perpendicular to the multilayer plane must be taken into consideration. We will analyze the Co_1/Pd_2 multilayer in two steps. In the first step, we neglect the spin-orbit interaction on the Pd atoms so that only the effect of hybridization between the Co and Pd levels and the repositioning of the Fermi energy are taken into account. In the second step, the effect of the large Pd spin-orbit coupling is considered. The analysis, though straightforward, is complicated by the large number of levels and high-symmetry $\mathbf{k}$ points which must be treated so that we will only outline the most important elements in what follows.

For the structure of the Co/Pd multilayers an ABC stacking sequence of [111] (close packed) planes of a fcc lattice was assumed. The crystal structure has trigonal symmetry (point group D_{3d}). It is convenient to choose the hexagonal lattice vectors as primitive vectors. The reciprocal lattice is then described by hexagonal lattice vectors as well, and the high-symmetry lines and points of the Brillouin zone are the same as those for the (periodically repeated) monolayer. The parameters in this pseudomorphic model for the multilayers were evaluated by total energy minimization as described in Ref. 10, using the full potential implementation[29] of the LAPW method.[18]

In Fig. 12 we show the anisotropy energy as a function of the Fermi energy, calculated using a grid of 9408 $\mathbf{k}$ points in the full BZ (solid curve). This grid corresponds to 28 divisions along the in-plane reciprocal lattice vectors and 12 divisions along the perpendicular reciprocal lattice vector and we call it, for short, a 28-28-12 grid. An oscillatory dependence on the band filling is found, and a maximum occurs at the actual Fermi energy, denoted by the vertical line. The sign of the anisotropy energy corresponds to a perpendicular magnetization. The dotted curve indicates the results of a calculation using a

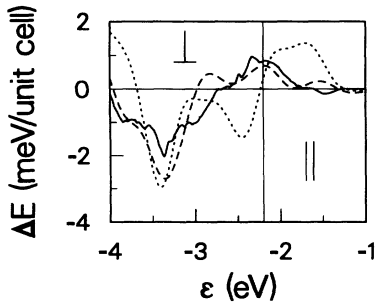

FIG. 12. Anisotropy energy curve of a Co_1/Pd_2 multilayer as a function of the energy, calculated using 28 and 12 divisions along the in-plane and perpendicular reciprocal lattice vectors, respectively (solid curve), 6 and 1 divisions (dotted curve), and 6 and 2 divisions (dashed curve). The latter two curves are broadened with a Gaussian with a width of 0.4 eV. The actual Fermi energy is denoted by the vertical line.

6-6-1 grid, which was broadened using a Gaussian with a width of 0.4 eV. Although an oscillatory dependence on the band filling is found, an in-plane anisotropy occurs over too large a region of the band filling. A calculation using a 6-6-2 grid, in which two divisions along the perpendicular reciprocal lattice vector were chosen, gives results in better agreement with the more extensive calculation. This shows that the dispersion of the energy bands in the $\mathbf{k}_z$ direction cannot be neglected.

We have examined the contributions to the anisotropy energy curve from the six $\mathbf{k}$ points Γ, K, M, A, H, and L. The latter three high-symmetry points correspond to the Γ, K, and M points with $k_z = \pi/c$. The anisotropy energy contributed by each $\mathbf{k}$ point is shown in Figs. 13 and 14; in Fig. 13, ξ_{Pd} has been set to zero. Adding the contributions of all $\mathbf{k}$ points, the dashed curves in Figs. 13(a) and 14(a) are obtained. Broadening the curves with a Gaussian of width 0.4 eV yields the dashed curves in Figs. 13(b) and 14(b), which have a similar functional dependence on the band filling as the full calculation, represented by the solid curves. At the actual Fermi energy in Fig. 14(b), the correspondence is not so good; this will be explained later. At each $\mathbf{k}$ point the position of the majority- and minority-spin d bands is indicated by arrows pointing downwards or upwards, respectively. Arrows at the top (bottom) of the panel indicate eigenstates which have more than 50% Pd (Co) character. Because of the low symmetry of the Bravais lattice (there is no mirror-plane parallel to the multilayer planes), the eigenstates contain, in general, a mixture of odd and even (in z) states. If an eigenstate has a dominant m partial wave character, the absolute value of m is indicated in the figure as well.

1. $\xi_{Pd} = 0$

If we compare the bottom panel of Fig. 8 (from -6 to -9 eV) with Fig. 13(b), then we see a striking similarity in the behavior of the anisotropy energy. Starting from an energy where all the d bands are filled, an in-plane magnetization is first found. At lower energies, perpendicular magnetization is preferred and at still lower energies, in-plane magnetization is again favored.

In Fig. 13(a), the preferred in-plane magnetization for $\varepsilon \sim -1.75$ eV arises from the interaction between anti-

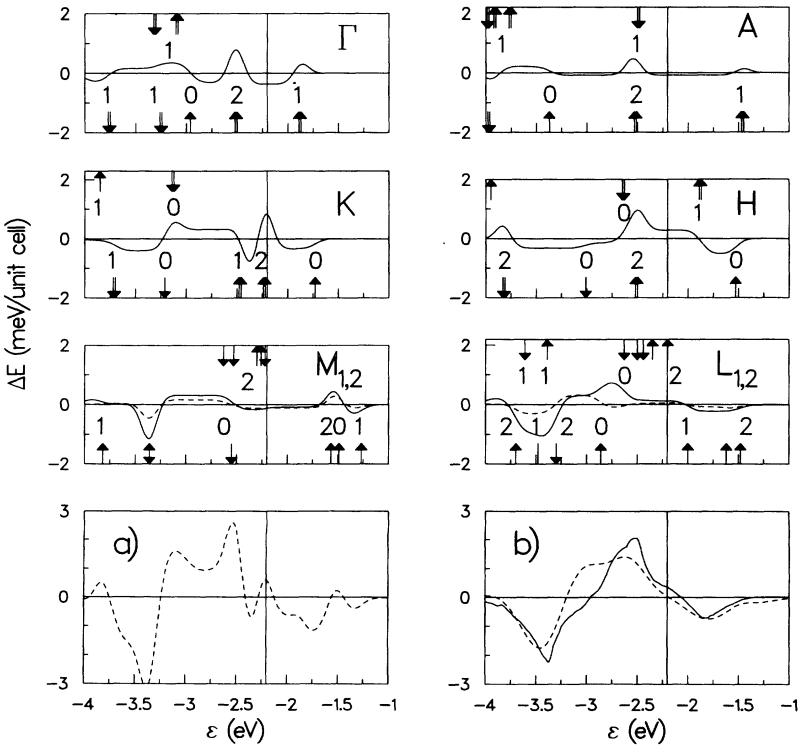

FIG. 13. Anisotropy energy of Co_1/Pd_2 contributed by the high-symmetry points Γ, K, M, A, H, and L as a function of energy corresponding to variable band filling. The Pd spin-orbit interaction has been switched off. The actual Fermi energy is denoted by the vertical line at -2.2 eV. Arrows at the top (bottom) of the panels indicate the position of the energy levels with predominant Pd (Co) character; a double arrow is used to denote degenerate eigenstates. Upward (downward) pointing arrows indicate minority- (majority-) spin eigenstates. The predominant m partial wave character is denoted by the labels where applicable. For the M and L points, the subscripts 1 and 2 refer to the solid and dashed curves, respectively. The dashed curve in (a) is the result of adding the contributions of these $\mathbf{k}$ points. The dashed curve in (b) is obtained by an additional broadening using a Gaussian with a width of 0.4 eV. The solid curve results from a calculation where 9408 ($= 28 \times 28 \times 12$) $\mathbf{k}$ points in the BZ were used.

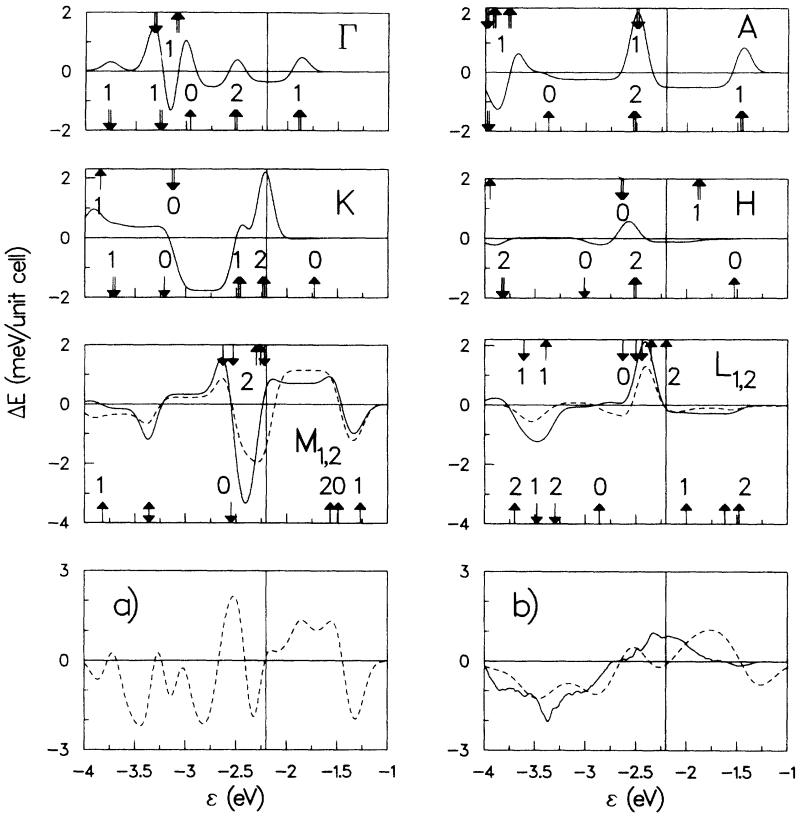

FIG. 14. Anisotropy energy of Co_1/Pd_2 contributed by the high-symmetry points Γ, K, M, A, H, and L as a function of energy corresponding to variable band filling. The Pd spin-orbit coupling parameter has been switched on. The labeling in the figure is the same as in Fig. 13.

bonding minority spin states with lower-lying minority spin states at K, H, and L.

For $\varepsilon \sim -2.5$ eV the dominant contribution to the preferred perpendicular magnetization comes from lifting the degeneracy of the Co $\pm 2 \uparrow$ states at Γ, A, and H. The positive plateau at $-3.25 < \varepsilon < -2.5$ comes from the coupling of even states of one spin with odd states of the opposite spin at K, M, and L.

For $-3.7 < \varepsilon < -3.25$ there are contributions favoring in-plane magnetization from the K, M, H, and L points. Part of this contribution comes from the coupling of even and odd states of the same spin (K and L), the rest comes from coupling between even states of opposite spin as well as from coupling between odd states of opposite spin (M, H, and L).

A more detailed comparison of the monolayer and multilayer is rendered difficult by the strong Co-Pd d-band overlap and strong hybridization; see the atom projected d densities of states in Fig. 15. At Γ, the ordering of the uppermost four states in Fig. 8 and Fig. 13 is the same. The anisotropy energy is similar but because the $\pm 2 \uparrow$ state has been pushed to higher energy in Co_1/Pd_2, a region where an in-plane magnetization is favored appears between the $0 \uparrow$ and $\pm 2 \uparrow$ states. In addition, the size of the contribution of Γ to the anisotropy energy has decreased by a factor 2 because of the reduced weight of Γ in the three-dimensional structure.

The effect of having a three-dimensional structure with Co_1/Pd_2 can be seen by comparing the level structure at Γ and A in Fig. 13. Although the ordering of the highest four levels is the same, the four levels at A are spread over an energy range which is almost twice as large as that at Γ. The second-order perturbation theory contributions to the anisotropy energy which scale inversely with the energy separation of the levels, are reduced correspondingly. As a result of the strong admixture of Pd character into the twofold degenerate states and of setting ξ_{Pd} to

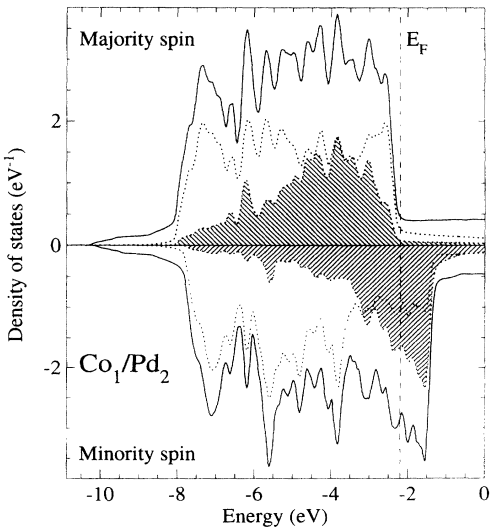

FIG. 15. Majority- and minority-spin densities of states for Co_1/Pd_2 in the absence of spin-orbit coupling. The solid line is the total state density for a given spin, the dotted lines are the Co and Pd d state densities. The Co d densities of states are shaded.

zero, the contributions favoring a perpendicular magnetization from lifting these degeneracies are reduced. The most important contribution from Γ and A to the total anisotropy energy is the peak at -2.5 eV favoring perpendicular magnetization, which results from lifting the degeneracy of the $\pm 2 \uparrow$ state.

At K the most significant change in the energy level structure of Co_1/Pd_2 compared to that of the Co monolayer is the displacement of the doubly degenerate $\pm 2 \uparrow$ level by hybridization with Pd so that it is positioned at the Fermi energy (corresponding to 29 valence electrons). The location of this degenerate state at the Fermi energy is confirmed by full potential calculations.[10] Because of the strong admixture of Pd d character and because ξ_{Pd} has been set to zero, the contribution of this state to the anisotropy energy is only moderate. When the Pd spin-orbit interaction is switched back on, however, we shall see that this state provides the single most important contribution to the perpendicular magnetization found in Co/Pd multilayers.

The interaction between the Co $0 \uparrow$ and $\pm 1 \uparrow$ states at K favors in-plane magnetization for $\varepsilon \sim -1.8$ eV. The interaction between the Co $0 \downarrow$ and $\pm 1 \downarrow$ states leads similarly to an in-plane contribution for $\varepsilon \sim -3.5$ eV. For $-3.2 < \varepsilon < -2.5$ eV, the interaction between the Co $0 \downarrow$ and $\pm 1 \uparrow$ states favors a perpendicular magnetization.

Although the contributions to the anisotropy energy from the H point in Fig. 13 are comparable to those from the other **k** points, when the Pd spin-orbit interaction is switched back on, all that remains is a small contribution favoring a perpendicular magnetization from lifting the degeneracy of the $\pm 2 \uparrow$ state which lies 0.3 eV below the Fermi energy.

The analysis of the contribution from the M point to the anisotropy energy of the Co monolayer was complicated by the lack of threefold symmetry and the resulting large number of nondegenerate eigenstates. The same is true of the M and L points for the Co_1/Pd_2 multilayer. The most important point to be noted is that the states close to the Fermi energy at these **k** points have mainly Pd character so that we expect a big change in anisotropy energy when the large Pd spin-orbit interaction $\xi_{Pd} \sim 0.2$ eV is switched on. The preference for in-plane magnetization for $\varepsilon \sim -1.75$ eV at L_1 comes from the interaction between the Co $|m| = 2 \uparrow$ and $|m| = 1 \uparrow$ states which straddle this energy. For $-3.25 < \varepsilon < -2.5$ eV, there are contributions both from M and L favoring a perpendicular magnetization. These contributions come from the coupling of even Co states of one spin with odd Co states of the opposite spin. The large contribution from the L_1 point to an in-plane magnetization for $-3.7 < \varepsilon < -3.25$ eV is largely attributable to the interaction between the Co $|m| = 2$ states of opposite spins.

2. $\xi_{Pd} \neq 0$

We now switch the spin-orbit interaction back on on the Pd atoms. Comparing Figs. 13 and 14 the most significant effect is that the peak at -2.5 eV in Fig. 13(b) is shifted to -2.25 eV in Fig. 14(b) to straddle the Fermi energy (corresponding to 29 valence electrons). The magnitude of the anisotropy energy at the Fermi level favoring perpendicular magnetization is thereby doubled. In the calculations based on the high-symmetry points only [dashed curves in Figs. 14(a) and 14(b)] this peak is placed too high in energy.

The anisotropy energy curves at Γ and A are qualitatively unchanged but the amplitudes have increased strongly. The largest changes can be seen to correlate quite well with the presence of states with predominantly Pd character.

At K the influence of the Pd spin-orbit interaction is very large. The most significant feature is the increase in the contribution at the Fermi energy favoring perpendicular magnetization which is directly attributable to the hybridization of the Co $\pm 2 \uparrow$ state with Pd d states which displaced it up to the Fermi energy. At lower energy, $-3.2 < \varepsilon < -2.5$ eV, an in-plane magnetization is favored and for $\varepsilon < -3.2$ eV, perpendicular magnetization. This reverses the situation in Fig. 13.

The effect of the Pd spin-orbit interaction on the situation at M is equally dramatic. The largest changes occur for $-2.8 < \varepsilon < -1.5$ eV and, as noted above, are directly related to the states with mainly Pd d character in this energy range. The plateau in the anisotropy energy for $-2.25 < \varepsilon < -1.5$ eV is an important contribution to the peak in the anisotropy energy at the Fermi level favoring perpendicular magnetization. The origin of this plateau can be fairly easily understood. The lowest Pd majority spin state shown at the top of the M panel has 13% d_{yz} ($|m| = 1$) and 19% d_{xy} ($|m| = 2$) character per Pd atom. The middle state of the three uppermost minority spin states shown at the bottom of the M panel has 13% $d_{3z^2-r^2}$ ($m = 0$) character per Pd atom. The energy separation between these two states is 1.2 eV. With $\xi_{Pd} = 0.23$ eV, we estimate a positive contribution of 0.7 meV favoring a perpendicular magnetization.

The net effect of the negative anisotropy below and the positive plateau above the Fermi energy at M is to displace the peak (favoring perpendicular magnetization) in the dashed curve from -2.75 eV in Fig. 13(b) to -1.75 eV in Fig. 14(b). Because the discrete states at Γ, A, K, H, M, and L in reality form bands (which is taken into account only very approximately by the Gaussian broadening) a smaller number of electrons actually contribute to the anisotropy energy in the calculation with a better Brillouin zone sampling. This effect explains the incorrect location of the maximum in the dashed anisotropy energy curve of Fig. 14(b).

Summarizing, the single most important contribution to the perpendicular magnetic anisotropy of Co/Pd multilayers is the presence of states close to the actual Fermi energy with mainly Co $d_{x^2-y^2}$ and d_{xy} character. These states are positioned at the Fermi energy by hybridization with the neighboring Pd atoms and their contribution to the anisotropy energy is enhanced by the resulting Pd character in the eigenstates and the large Pd spin-orbit interaction.

B. Co_1/Ag_2

A comparison between the anisotropy energies of Co_1/Ag_2 and Co_1/Pd_2 multilayers is interesting because

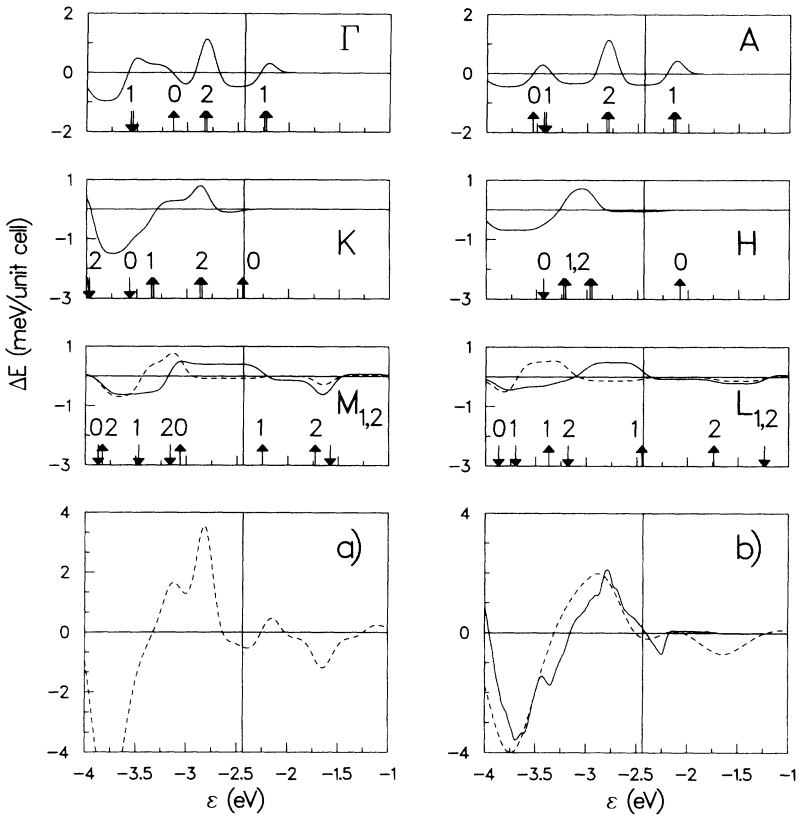

FIG. 16. Anisotropy energy of Co_1/Ag_2 contributed by the high-symmetry points as a function of the energy. The labeling in the figure is the same as in Fig. 13.

unlike the Co monolayer and in common with Co_1/Pd_2, Co_1/Ag_2 has a perpendicular anisotropy even though it is much smaller than that of Co_1/Pd_2.[10] In Fig. 16 the anisotropy energy curve is shown calculated using a 28-28-12 grid [solid curve in Fig. 16(b)], and analyzed in contributions from the high-symmetry points. The center of the Ag majority-spin d bands is 2.7 eV below that of the Co majority-spin d bands and the Ag and Co bandwidths are 3.4 and 2 eV, respectively, so that the Ag and Co majority-spin d bands are separated by an energy gap; see the atom projected densities of states in Fig. 17. The minority-spin band centers are separated by even more, 4.1 eV, and because the bandwidths are essentially the same the gap between Ag and Co minority spin d bands is even larger. As a result, all eigenstates shown in Fig. 16 have predominantly Co character, with only a little Ag d character mixed in by hybridization. The effect of the large Ag spin orbit is correspondingly reduced and the amplitudes of the anisotropy energy curve at the separate $\mathbf{k}$ points are smaller than in Co_1/Pd_2. If the Ag spin-orbit interaction is switched off, the anisotropy energy at the actual Fermi energy is only reduced by 0.06 meV. Compared to Co_1/Pd_2 the actual Fermi energy (corresponding to 31 valence electrons) is at a higher energy in the Co d band structure. Compared to the Co monolayer, however, it is much closer to the energies of the $d_{x^2-y^2}$ and d_{xy} eigenstates which are largely responsible for the positive amplitude in the anisotropy energy curve. It is therefore concluded that the smaller perpendicular anisotropy energy of Co_1/Ag_2 multilayers (compared to Co_1/Pd_2) is due to a larger band filling in the Co d band structure as well as to a reduced Ag d and Co d hybridization. Nevertheless, a perpendicular orientation of the magnetization is found because the actual Fermi energy lies lower with respect to the important Co d bands than in the monolayer.

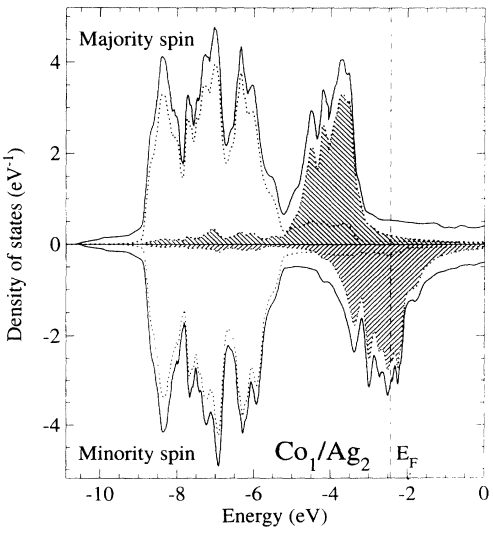

FIG. 17. Majority- and minority-spin densities of states for Co_1/Ag_2 in the absence of spin-orbit coupling. The solid line is the total state density for a given spin, the dotted lines are the Co and Ag d state densities. The Co d densities of states are shaded.

VI. CONCLUSIONS

We have shown that the anisotropy energy curves of a Co monolayer and Co_1/Pd_2 and Co_1/Ag_2 multilayers can be largely understood by analyzing the eigenstates and energy bands at a few high-symmetry points in the BZ only. The anisotropy energy was found to oscillate with the band filling in all cases. The most important factors leading to perpendicular magnetic anisotropy in the Co_1/X_2 multilayers were found to be (i) the position of the Fermi energy close to doubly degenerate states with mainly Co $d_{x^2-y^2}$ and d_{xy} character, (ii) strong hybridization between Co d states which have a large exchange splitting but a small spin-orbit interaction and X d states which have a small exchange splitting but a large spin-orbit interaction.

The Co_1/Pd_2 multilayer is found to be particularly favorable because there is a large overlap and hybridization between the Co and Pd d bands and the total number of valence electrons is such that the Fermi energy is located at the maximum in the anisotropy energy curve calculated as a function of the band filling. The smaller magnetic anisotropy energy of Co_1/Ag_2 compared to Co_1/Pd_2 is caused by a larger band filling as well as a smaller hybridization between Co and Ag d states.

[1] P. F. Carcia, A. D. Meinhaldt, and A. Suna, Appl. Phys. Lett. **47**, 178 (1985).

[2] H. J. G. Draaisma, W. J. M. de Jonge, and F. J. A. den Broeder, J. Magn. Magn. Mater. **66**, 351 (1987).

[3] F. J. A. den Broeder, W. Hoving, and P. J. H. Bloemen, J. Magn. Magn. Mater. **93**, 562 (1991), and references therein.

[4] L. Néel, J. Phys. Rad. **15**, 225 (1954).

[5] P. Bruno, J. Phys. F **18**, 1291 (1988).

[6] A. J. Bennett and B. R. Cooper, Phys. Rev. B **3**, 1642 (1971); H. Takayama, K. P. Bohnen, and P. Fulde, *ibid.* **14**, 2287 (1976); M. Kolar, Phys. Status Solidi B **96**, 683 (1979). Studies based on tight-binding Hamiltonians have been carried out more recently by P. Bruno, Phys. Rev. B **39**, 865 (1989); S. Pick and H. Dreysse, *ibid.* **46**, 5802 (1992).

[7] J. Friedel, in *The Physics of Metals*, edited by J. M. Ziman (Cambridge University Press, Cambridge, 1969).

[8] C. Chappert and P. Bruno, J. Appl. Phys. **64**, 5736 (1988).

[9] R. M. Jungblut, M. T. Johnson, J. aan de Stegge, A. Reinders, and F. J. A. den Broeder, J. Appl. Phys. **75**, 6424 (1994).

[10] G. H. O. Daalderop, P. J. Kelly, and M. F. H. Schuurmans, Phys. Rev. B **42**, 7270 (1990); in *Science and Technology of Nanostructured Magnetic Materials, NATO Advanced Study Institute Series*, edited by G. C. Hadjipanayis and G. A. Prinz (Plenum, New York, 1991), p. 185.

[11] G. H. O. Daalderop, P. J. Kelly, and F. J. A. den Broeder, Phys. Rev. Lett. **68**, 682 (1992).

[12] K. Kyuno, R. Yamamoto, and S. Asano, J. Phys. Soc. Jpn. **61**, 2099 (1992); P. J. Kelly and G. H. O. Daalderop, J. Magn. Soc. Jpn. **17**, 728 (1993).

[13] R. H. Victora and J. M. MacLaren, Phys. Rev. B **47**, 11583 (1993).

[14] G. Y. Guo, W. M. Temmerman, and H. Ebert, J. Phys.: Condens. Matter **3**, 8205 (1991); J. Magn. Magn. Mater. **104-107**, 1772 (1992).

[15] Various first-principles (local-density-approximation) calculations of the MAE for free-standing transition metal monolayers, bilayers, and overlayers have been reported: J. G. Gay and R. Richter, Phys. Rev. Lett. **56**, 2728 (1986); J. Appl. Phys. **61**, 3362 (1987); W. Karas, J. Noffke, and L. Fritsche, J. Chim. Phys. Phys.-Chim. Biol. **86**, 861 (1989); C. Li, A. J. Freeman, and C. L. Fu, Phys. Rev. B **42**, 5433 (1990); I. V. Solov'ev, Phys. Met. Metallography **75**, 120 (1993); D. S. Wang, R. Wu, and A. J. Freeman, Phys. Rev. Lett. **70**, 869 (1993); Phys. Rev. B **47**, 14932 (1993).

[16] G. H. O. Daalderop, P. J. Kelly, and M. F. H. Schuurmans, Phys. Rev. B **41**, 11919 (1990).

[17] P. Hohenberg and W. Kohn, Phys. Rev. **136**, B864 (1964); W. Kohn and L. J. Sham, *ibid.* **140**, A1133 (1965). More recent references are given by O. Gunnarsson and R. O. Jones, Rev. Mod. Phys. **61**, 689 (1989).

[18] O. K. Andersen, Phys. Rev. B **12**, 3060 (1975).

[19] We have studied the effect of iterating the Hamiltonian including spin-orbit coupling to self-consistency considering the change of magnetization direction as the perturbation. For the systems which we have considered this more computationally demanding procedure does not lead to different anisotropy energies.

[20] A. R. Mackintosh and O. K. Andersen, in *Electrons at the Fermi Surface*, edited by M. Springford (Cambridge University Press, Cambridge, 1980); M. Weinert, R. E. Watson, and J. W. Davenport, Phys. Rev. B **32**, 1215 (1985).

[21] E. Abate and M. Asdente, Phys. Rev. **140**, A1303 (1965).

[22] J. F. Janak, Phys. Rev. B **16**, 255 (1977); O. Gunnarsson, Physica B+C (Amsterdam) **91**, 329 (1977).

[23] O. Jepsen, J. Madsen, and O. K. Andersen, Phys. Rev. B **26**, 2790 (1982).

[24] Because we use the atomic-sphere approximation in combination with an *ABC* stacking sequence and repeated slab approximation, the mirror symmetry is, in principle, broken; in practice, the mixing of even and odd states turns out to be negligible.

[25] This is discussed for Ni by R. Gersdorf, Phys. Rev. Lett. **40**, 344 (1978).

[26] This need not be true in general. The number of **k** points which needs to be examined in order to reproduce the "exact" results calculated with a large number of sampling points depends on the subjective judgement as to what constitutes qualitative agreement.

[27] G. H. O. Daalderop, P. J. Kelly, and M. F. H. Schuurmans, Phys. Rev. B **44**, 12054 (1991).

[28] V. Heine and J. H. Samson, J. Phys. F **10**, 2609 (1980); **13**, 2155 (1983); V. Heine, W. C. Kok, and C. M. M. Nex, J. Magn. Magn. Mater. **43**, 61 (1984).

[29] H. J. F. Jansen and A. J. Freeman, Phys. Rev. B **29**, 5965 (1984).